

# The possible ubiquity of energy injection in Gamma-Ray Burst afterglows

A. Panaitescu and W.T. Vestrand

*ISR-2: Space and Remote Sensing, MS B244, Los Alamos National Laboratory, Los Alamos, NM 87545, USA*

## ABSTRACT

Since its launch in 2004, the Swift satellite has monitored the X-ray afterglows of several hundred Gamma-Ray Bursts, and revealed that their X-ray light-curves are more complex than previously thought, exhibiting up to three power-law segments. Energy injection into the relativistic blast-wave energizing the burst ambient medium has been proposed most often to be the reason for the X-ray afterglow complexity. We examine 117 light-curve breaks of 98 Swift X-ray afterglows, selected for their high-quality monitoring and well-constrained flux decay rates. Thirty percent of afterglows have a break that can be an adiabatic jet-break, in the sense that there is one variant of the forward-shock emission from a collimated outflow model that can account for both the pre- and post-break flux power-law decay indices, given the measured X-ray spectral slope. If allowance is made for a steady energy injection into the forward-shock, then another 56 percent of X-ray afterglows have a light-curve break that can be explained with a jet-break. The remaining 12 percent that are not jet-breaks, as well as the existence of two breaks in 19 afterglows (out of which only one can be a jet-break), suggest that some X-ray breaks arise from a sudden change in the rate at which energy is added to the blast-wave, and it may well be that a larger fraction of X-ray light-curve breaks are generated by that mechanism. The fractional increase in the shock energy, inferred from the energy injection required to account for the observed X-ray flux decays, may be anticorrelated with the GRB prompt output, whether the X-ray break is a jet-break or an energy-injection break. That anticorrelation can also be seen as bursts with a higher energy output being followed by faster fading X-ray afterglows. To test the above two mechanisms for afterglow light-curve breaks, we derive comprehensive analytical results for the dynamics of outflows undergoing energy injection and for their light-curves, including closure relations for inverse-Compton afterglows and for the emission from spreading jets interacting with an wind-like ambient medium.

**Key words:** radiation mechanisms: non-thermal, relativistic processes, shock waves, gamma-ray bursts, ISM: jets and outflows

## 1 INTRODUCTION

The power-law temporal decays displayed by the radio, optical, and X-ray fluxes of GRB afterglows ( $F_\nu \propto t^{-\alpha}$ ) have provided strong support for the prediction (Meszaros & Rees 1997) that afterglows arise from the relativistic blast-wave generated as the GRB outflow ejecta interacts with the ambient medium. If the GRB outflow is a collimated jet then a break in the smooth power-law decay of the afterglow is expected for both either a conical jet (Panaitescu, Meszaros & Rees 1998) or a sideways-spreading jet (by Rhoads 1999). The breaks found in the flux decay light curves of most of the well-sampled afterglows that were localized by the BeppoSAX satellite seemed to provide solid observational support for the existence of these predicted jet-breaks (e.g. Frail et al 2001).

It was also realized early on that there should be a substantial diversity in the steepness of the afterglow flux decay, even when the spectral slope is constant, if the fundamental forward-shock parameters vary as the shock traverses the ambient medium. Rees & Meszaros (1998) derived the expected power-law flux decay for the forward-shock synchrotron flux in the case of an outflow whose kinetic energy-per-solid angle  $dE/d\Omega$  is not constant in time, either because the shock's energy increases due to fresh ejecta arriving at the blast-wave or because  $dE/d\Omega$  is anisotropic. Two important microphysical parameters ( $\epsilon_e$  and  $\epsilon_B$ ), which quantify the fraction of the post-shock energy acquired by electrons and magnetic field, also determine the intensity the afterglow synchrotron flux, and their variability could also yield a variety of decay indices  $\alpha$ .

Swift measurements of GRB X-ray afterglows provide support for that shock parameters vary. The standard forward-shock model with constant energy and shock micro-parameters predicts a closure relation between the temporal decay index  $\alpha$  and the slope  $\beta$  of the X-ray continuum ( $F_\nu \propto \nu^{-\beta}$ ) of the form  $\alpha = 1.5\beta + \text{const}$ . The early X-ray flux of some Swift afterglows decays slower than expected for the measured spectral slope  $\beta$ , which was attributed to a variable kinetic energy of the forward shock (Nousek et al 2006, Panaitescu et al 2006, Zhang et al 2006). Moreover, the flux decay indices  $\alpha$  displayed by Swift X-ray afterglows after the slow decay phase are not correlated with the X-ray spectral slope  $\beta$  (Panaitescu 2007), as would be expected from the  $\alpha - \beta$  closure relation for the forward-shock emission.

When optical light-curves are taken into account, the standard jet model fares even worse, being inconsistent with practically all Swift afterglows (Liang et al 2008). While more than half of the well-sampled optical afterglows display coupled optical and X-ray light-curves (Panaitescu & Vestrand 2011), exhibiting similar flux decay indices and/or simultaneous light-curve breaks, many other afterglows show a decoupling of their optical and X-ray light-curves, with a light-curve break occurring only in the X-ray. At least four possibilities for this light-curve decoupling, which is not predicted by the standard jet model, have been proposed: *i*) the X-ray afterglow emission arises occasionally from the same not-yet-understood mechanism which produces the prompt burst emission (Ghisellini et al 2007), *ii*) there is a dominant contribution of the reverse-shock to the afterglow emission (Uhm & Beloborodov 2007), *iii*) the forward-shock emission is reprocessed by bulk-scattering and/or inverse-Compton scattering outside the forward-shock (Panaitescu 2008), or *iv*) the optical and X-ray afterglow flux arise from different parts of the forward-shock, from different jets (e.g. Racusin et al 2008).

In this work, we assume that Swift X-ray afterglows arise from the forward-shock, and attribute the failure of the standard jet model in accounting for the X-ray flux decay indices to the assumption that the forward shock energy is constant.

Evolving micro-physical parameters (e.g. Ioka et al 2006) could, in principle, explain the measured X-ray flux decay indices, but the existence of light-curve breaks requires an unnatural, sudden change in their evolution. For that reason, we maintain in this work the basic assumption of the standard jet model that micro-physical parameters do not evolve.

We also assume that the ambient medium with which the post-GRB outflow interacts is uniform, without discontinuities that could yield breaks in the afterglow light-curve at a frequency. A notable model thus excluded is that where the afterglow-producing outflow interacts with a prior outflow (Ioka et al 2006) whose density increases radially outward up to its termination shock, yielding a slower decay of the afterglow flux than expected for a homogeneous ambient medium, followed by a break to a steeper decay.

One reason for relaxing the constant shock energy constraint is the observational evidence for X-ray flares in Swift afterglows (e.g. Chincarini et al 2007). The short timescale

of those flares indicates that the GRB progenitor produces relativistic ejecta after the burst phase, whose arrival at the decelerating forward-shock could increase substantially the blast-wave's energy. Our hypothesis is that such an injection of energy in the forward-shock is, in general, a more persistent and continuous process. However, we note that the fluence of X-ray flares is about 10 percent that of the burst (Falcone et al 2007), hence the late outflow powering the flares could carry a dynamically-important energy only if that outflow is much less efficient than the GRB outflow in producing X-ray emission.

We derive in §2 the closure relations  $\alpha - \beta$  for a continuous energy injection in the forward-shock. For the ease of extracting from observations the required injected power history, we assume that the forward-shock energy increases as a power with observer-time,  $E \propto t^e$ , which is motivated by that the resulting afterglow flux should be power-law in observer time. This assumption circumvents a calculation of the kinematics for the ejecta – forward-shock interaction.

In §3, the closure relations for the forward-shock emission with energy injection are applied to a set of Swift afterglows with well sampled light-curves. There, we examine two plausible scenarios for the origin of afterglow X-ray light-curve breaks (break in energy injection, jet-break), three dynamical regimes of the forward-shock (spherical expansion, conical jet, spreading jet), and two radiation processes that may yield the afterglow X-ray flux (synchrotron, inverse-Compton).

## 2 ANALYTICAL FLUX DECAYS FOR FORWARD-SHOCK MODELS WITH ENERGY INJECTION

There are three mechanisms that could produce a change in the flux power-law decay index  $\alpha$ , i.e. an afterglow light-curve break.

(1) Passage of a spectral break. X-ray light-curve breaks are, generally, not accompanied by a spectral evolution (Nousek et al 2006; Liang, Zhang & Zhang 2007; Willingale et al 2007), hence their origin in the passage of the spectral feature is largely ruled out, but there are other reasons why such an X-ray light-curve break origin is unlikely. The slower evolution of the cooling frequency  $\nu_c$  (the synchrotron characteristic frequency at which radiate the electrons that cool radiatively on the hydrodynamical timescale) leads to extended X-ray light-curve breaks when  $\nu_c$  crosses the 0.3-10 keV band. The peak frequency  $\nu_i$  of the  $\nu F_\nu$  synchrotron spectrum decreases faster, but it is likely to be lower than the X-rays even at early times, hence it cannot cross the X-ray band during afterglow observations.

(2) Jet-break. A light-curve break occurs at the ‘jet-break time’, when the outflow Lorentz factor  $\Gamma$  drops below the inverse of the jet half-angle  $\theta_j$ . For a ‘conical jet’ that does not spread laterally (as in the case of an outflow core embedded in an envelope that prevents the spreading of the core but yields a negligible emission), the steepening of the X-ray flux decay is solely due to that, after the jet-break time, the average kinetic energy per solid angle  $dE/d\Omega$  over the visible cone of angle  $\theta = \Gamma^{-1}$  (where relativistic Doppler

boost is effective) is decreasing with observer-frame time. For a ‘spreading jet’ (as expected for a top-hat distribution of  $dE/d\Omega$ ), in addition to the above-described geometrical-relativistic effect, there is a second contribution to the X-ray flux decay steepening from the enhanced jet deceleration produced by the jet lateral spreading.

(3) Energy injection break. If energy injection occurs routinely in GRB afterglows, then a light-curve break could be produced by a change in the injected power. The dynamical behaviours of the forward-shock model to be considered are: *i*) a ‘spherical’ outflow, i.e. a wide jet whose edge becomes visible to the observer after the last X-ray measurement (at  $t_{\text{end}}$ ), which occurs if jet half-angle satisfies  $\theta_j > 1/\Gamma(t_{\text{end}})$ , and *ii*) a narrow jet whose edge is already visible at the first X-ray observation (at  $t_{\text{start}}$ ), occurring when  $\theta_j < 1/\Gamma(t_{\text{start}})$ . For the latter model, we will consider both a conical jet and a spreading jet. These dynamical models are applicable also to X-ray afterglows without light-curve breaks, in which case the energy injection law must be unevolving (a single index  $e$ ).

We will investigate the ability of the energy-injection break and jet-break models above to accommodate the observed X-ray flux decays before and after the break, with allowance for all three dynamical models (spherical outflow, conical jet, spreading jet), for two types of ambient medium (homogeneous and wind-like), two radiation mechanisms dominating the X-ray flux (synchrotron and inverse-Compton), and two possible locations of the X-ray relative to the cooling frequency  $\nu_c$  but, first, a word about their rationale.

Wind-like media, having a  $n \sim 0.1 - 1 (r/10^{18} \text{ cm})^{-2}$  particle density, are expected at 0.1-1 pc from the source of long GRBs, i.e. where the 100s – 1Ms afterglow emission is produced, because the progenitors of such bursts are massive Wolf-Rayet stars that drive powerful winds. The termination-shock of such winds is of several pcs (Garcia-Segura et al 1996), thus a homogeneous medium at the afterglow location seems unjustified. However, if the GRB progenitor resides in a highly-pressurized bubble, the wind termination-shock radius could be as low as 0.5 pc (Chevalier et al 2004), with a further reduction of that radius if the WR wind is weak, as expected along the rotation axis (Ramirez-Ruiz et al 2005), or if the WR star moves sufficiently fast relative to the ISM (van Marle et al 2006), thus the afterglow could occur in shocked wind, which is quasi-homogeneous.

Synchrotron emission is generally believed to produce all the afterglow emission, but the likelihood of inverse-Compton emission being dominant is higher at higher photon frequency, like X-rays. Admittedly, that requires a high environment density, perhaps ten times higher (Panaitescu 2011) than implied by the mass-loss rates and terminal wind velocities measured for Galactic Wolf-Rayet winds (Nugis & Lamers 2000).

## 2.1 Spectral characteristics

The  $\alpha$ – $\beta$  closure relations expected for a given variant of the forward-shock model are derived from the evolution of the spectral characteristics  $F_p$  (peak flux),  $\nu_i$  (frequency of the

$\nu F_\nu$  spectrum peak), and  $\nu_c$  (cooling frequency), and from the shape of the  $F_\nu$  spectrum at frequencies higher than its  $\min(\nu_i, \nu_c)$  peak:  $F_\nu \propto \nu^{-1/2}$  for  $\nu_c < \nu < \nu_i$ ,  $F_\nu \propto \nu^{-(p-1)/2}$  for  $\nu_i < \nu < \nu_c$  and  $F_\nu \propto \nu^{-p/2}$  for  $\max(\nu_i, \nu_c) < \nu$ , where  $p$  is the power-law index of the electron distribution with energy produced by the shock ( $dN/d\varepsilon \propto \varepsilon^{-p}$ ). Therefore, the flux received at observing frequency  $\nu$  satisfies  $F_\nu \propto F_p \nu_i^{(p-1)/2}$  for  $\nu_i < \nu < \nu_c$  and  $F_\nu \propto F_p \nu_i^{(p-1)/2} \nu_c^{1/2}$  for  $\max(\nu_i, \nu_c) < \nu$  ( $\nu_c < \nu < \nu_i$  implies an X-ray spectrum with  $\beta_x = 1/2$  that is harder than measured for nearly all Swift X-ray afterglows).

For a spherical outflow (or a jet before the jet-break time  $t_j$ ) and for synchrotron emission,  $F_p \propto BM\Gamma$ ,  $\nu_i \propto \gamma_i^2 B\Gamma$ ,  $\nu_c \propto \gamma_c^2 B\Gamma$ . Here  $M$  is the mass of the ambient medium swept-up by the forward-shock (i.e. the number of radiating electrons);  $B \propto (\epsilon_B n)^{1/2} \Gamma$  is the post-shock magnetic field, whose energy density  $B^2/(8\pi)$  is assumed to be a fraction  $\epsilon_B$  of the post-shock energy density  $u' = 4\Gamma^2 n m_p c^2$  (from the shock jump conditions);  $n$  is the external density at the shock’s location;  $\gamma_i \propto \epsilon_e \Gamma$  is the typical electron random Lorentz factor, parametrized as a fraction  $\epsilon_e$  of the proton random Lorentz factor  $\gamma_p \simeq \Gamma$ ; and  $\gamma_c \propto [B^2 t' (Y+1)]^{-1}$  is the random Lorentz factor of the electrons whose radiative cooling timescale equals the comoving-frame shock’s age  $t' = \int dr/(c\Gamma)$ ,  $r$  being the outflow radius and  $Y$  the Compton parameter. We assume the more likely situations of either electrons cooling mostly through synchrotron emission ( $Y < 1$ ) or, if inverse-Compton is dominant ( $Y > 1$ ), that  $\nu_c < \nu_i$ , in which case  $Y \simeq (\epsilon_e/\epsilon_B)^{1/2}$  is constant and does not affect the evolution of  $\nu_c$ .

For a jet (conical or spreading) after the jet-break time and for synchrotron emission, we have  $F_p \propto BM\Gamma^3$ , with  $\nu_i$  and  $\nu_c$  as above. Thus

$$F_p^{(\text{syn})} \propto \begin{cases} \sqrt{n} M \Gamma^2 & (t < t_j) \\ \sqrt{n} M \Gamma^4 & (t > t_j) \end{cases} \quad (1)$$

$$\nu_i^{(\text{syn})} \propto \sqrt{n} \Gamma^4 \quad (2)$$

$$\nu_c^{(\text{syn})} \propto (n^{3/2} \Gamma^2 t'^2)^{-1} \quad (3)$$

The characteristics of the *inverse-Compton* spectrum are immediately related with those of the synchrotron spectrum:  $F_p^{(\text{iC})} \simeq \tau_{\text{el}} F_p^{(\text{syn})}$  (where  $\tau_{\text{el}} \propto M/r^2$  is the optical thickness to electron scattering of the shocked ambient medium),  $\nu_i^{(\text{iC})} \simeq \gamma_i^2 \nu_i^{(\text{syn})}$ , and  $\nu_c^{(\text{iC})} \simeq \gamma_c^2 \nu_c^{(\text{syn})}$ , thus

$$F_p^{(\text{iC})} \propto \frac{M}{r^2} F_p^{(\text{syn})} \quad (4)$$

$$\nu_i^{(\text{iC})} \propto \sqrt{n} \Gamma^6 \quad (5)$$

$$\nu_c^{(\text{iC})} \propto (n^{7/2} \Gamma^6 t'^4)^{-1} \quad (6)$$

## 2.2 Outflow dynamics

The above equations for the spectral characteristics show that their evolution and, thus, the resulting flux decay index  $\alpha$ , is set by the forward-shock dynamics:  $\Gamma(t)$ ,  $M(t)$ , and  $r(t)$ . The energy-per-particle behind that shock is  $\epsilon/n' = \Gamma$ , hence the lab-frame energy of the forward-shock is  $\Gamma^2 M c^2$  and its dynamics is given by  $\Gamma^2 M = E/c^2 = (M_0 \Gamma_0)(t/t_0)^\epsilon$ ,

where  $M_0\Gamma_0$  is the kinetic energy of the ejecta (all transferred to the forward-shock) at the time  $t_0$  when the assumed power-law energy injection ( $E \propto t^e$ ) begins. The other equations for the forward-shock dynamics are  $dM = Ar^{-s}(r\theta)^2 dr$ , with  $\rho = Ar^{-s}$  the density of the ambient medium at radius  $r$  ( $s = 0$  for a homogeneous medium,  $s = 2$  for a wind) and  $d\theta = c_s dt'/r = dr/(\sqrt{3}r\Gamma)$  the increase of the jet opening at the comoving-frame sound speed ( $c_s = c/\sqrt{3}$ ), and  $dt = dr/(c\Gamma^2)$  for the observer-frame arrival time  $t$  of photons emitted along the direction toward the observer.

Defining  $f = M/M_0$ ,  $x = r/\tilde{r}$  with  $\tilde{r} \equiv (6M_0\Gamma_0/\pi A)^{1/(3-s)}$  (the radius where the lateral spreading almost doubles the initial opening of an adiabatic jet interacting with a homogeneous medium), and  $\tau = t/t_0$ , the above equations for the outflow dynamics become:

$$\Gamma^2 = \frac{\Gamma_0}{f} \tau^e \quad (7)$$

$$\frac{df}{dx} = 6\Gamma_0 x^{2-s} \theta^2 \quad (8)$$

$$\frac{d\theta}{dx} = \frac{1}{\sqrt{3}x\Gamma} \quad (9)$$

$$\frac{d\tau}{dx} = \frac{\tilde{r}}{2ct_0\Gamma^2} \quad (10)$$

Equation (10) allows the conversion of the jet dynamics  $[\Gamma(r), M(r), \theta(r)]$  from lab frame to observer frame  $[\Gamma(t), M(t), \theta(t)]$ .

For a spherical outflow, a conical jet, or a spreading jet before the jet-break time,  $\theta$  is constant and the above equations can be solved easily, leading to

$$\Gamma \propto t^{-(3-s-e)/(8-2s)} \quad (11)$$

$$M \propto t^{(3-s)(1+e)/(4-s)} (\propto nr^3) \quad (12)$$

$$r \propto t^{(1+e)/(4-s)} \quad (13)$$

$$t' \propto t^{(5-s+e)/(8-2s)} (\propto r/\Gamma) \quad (14)$$

which can be replaced in the equations for the synchrotron and inverse-Compton spectral characteristics (equations 1–3 and 4–6) to obtain their evolutions and, then, the power-law index of the afterglow flux decays given in lines 1, 2, 4, and 5 of Table 1 and Table 2, respectively.

## 2.3 Spreading jets

### 2.3.1 Adiabatic jet, homogeneous medium

For a jet spreading laterally, the dynamics equations can be solved analytically in the case of no energy injection and for a homogeneous medium. That has been done by Rhoads (1999), who obtained an exponential jet deceleration for a lateral spreading given by  $\theta = c_s t'/r$ :  $\Gamma \propto \exp(-kr)$ ,  $\theta \propto \exp(kr)/r$ ,  $f \propto \exp(2kr)$  at  $r > k^{-1}$ , where  $k = 1/\tilde{r}$ . Because the differential lateral spreading is “on top” of a conical jet and not “over” a cylindrical jet (as in Rhoads’ formalism), the correct lateral expansion is  $d\theta = c_s dt'/r$ . For  $e = 0$

and  $s = 0$ , equations (7)–(10) (which use the latter prescription for jet spreading) have the solution  $\Gamma \propto \exp(-kr)/r$ ,  $\theta \propto \exp(kr)$ ,  $f \propto r^2 \exp(2kr)$  for  $r > \tilde{r}$ , which can be shown to lead to the same flux power-law decay indices as for Rhoads’ prescription because the increase of the jet radius is only logarithmic in observer time (note that, for a nearly constant jet radius  $r$ ,  $d\theta = c_s dt'/r$  implies  $\theta = c_s t'/r$ ).

The above exponential solutions for the dynamics of an adiabatic jet interacting with a homogeneous medium can be expressed in observer time by integrating  $t = t(\tilde{r}) + \int_{\tilde{r}}^r dr/(2c\Gamma^2)$ , which leads to  $t \simeq \tilde{r}/(4c\Gamma^2)$  for  $r \gg \tilde{r}$ . Thus

$$\Gamma = \frac{1}{2} \left( \frac{\tilde{r}}{ct} \right)^{1/2} \propto \left( \frac{E}{n} \right)^{1/6} t^{-1/2} \quad (15)$$

from where it can be shown that

$$M = \frac{4Et}{\tilde{r}c} \propto E^{2/3} n^{1/3} t \quad (16)$$

$$\theta = \frac{2}{r} \left( \frac{1}{3} \tilde{r} ct \right)^{1/2} \propto \left( \frac{E}{n} \right)^{1/6} \frac{t^{1/2}}{r} \quad (17)$$

$$t' \simeq \frac{\tilde{r}}{c\Gamma} = 2 \left( \frac{\tilde{r}t}{c} \right)^{1/2} \propto \left( \frac{E}{n} \right)^{1/6} t^{1/2} \quad (18)$$

where  $E$  is the jet energy and  $\tilde{r} = (6E/\pi n m_p c^2)^{1/3}$ .

### 2.3.2 Energized jets

In the more general case of energy injection and/or for a wind-like medium, the solution to the dynamics equations (7)–(10) cannot be found analytically. They can be cast as logarithmic derivatives

$$\frac{d \ln f}{d \ln \tau} \propto \frac{\theta^2}{f^2} x^{2-s} \tau^{e+1} \quad (19)$$

$$\frac{d \ln \theta}{d \ln \tau} \propto \frac{\tau^{1+e/2}}{\sqrt{f}\theta x} \quad (20)$$

$$\frac{d \ln x}{d \ln \tau} \propto \frac{\tau^{e+1}}{fx} \quad (21)$$

and integrated numerically, which showed that the left-hand sides are (asymptotically) constant, i.e. the dynamics  $[M(t), \theta(t), r(t)]$  of a spreading jet undergoing energy injection according to  $E \propto t^e$  is a power-law in observer time. That dynamics is between the extreme cases of an adiabatic jet interacting with a homogeneous medium (which yields the fastest deceleration) and a spherical outflow with energy injection (which yields the slowest deceleration). Given that, in both of those two extreme cases, the dynamical quantities have a power-law evolution with time, it is not surprising that an intermediate case manifests that feature too.

Replacing power-law solutions for  $f$ ,  $\theta$ , and  $x$  in equations (19)–(21), allows the calculation of the temporal exponents by requiring that the right-hand sides are also constants, i.e. without a  $\tau$  dependence. The result is

$$M \propto t^{e+1-\frac{e}{3-s}} (\propto nr^3 \theta^2) \quad (22)$$

$$\theta \propto t^{\frac{1}{2}(1-\frac{e}{3-s})} \quad (23)$$

**Table 1.** Evolution of the spectral characteristics ( $F_p$  = spectral peak flux,  $\nu_i$  = energy at which radiate the electrons with typical post-shock energy,  $\nu_c$  = cooling frequency) with observer time  $t$  for the (synchrotron and inverse-Compton spectra, for two types of ambient media (homogeneous and  $r^{-2}$  wind), for three models for the forward-shock dynamics (‘spherical’ = wide jet, with a jet-break after last observation, ‘conical jet’ = confined jet, observed after jet-break, ‘spreading jet’ = laterally spreading jet, observed after jet-break), and a forward-shock energy increasing as  $E \propto t^e$ .

MODEL	HOMOGENEOUS MEDIUM			WIND-LIKE MEDIUM		
	$d \ln F_p / d \ln t$	$d \ln \nu_i / d \ln t$	$d \ln \nu_c / d \ln t$	$d \ln F_p / d \ln t$	$d \ln \nu_i / d \ln t$	$d \ln \nu_c / d \ln t$
syn – spherical	$e$	$-\frac{1}{2}(3 - e)$	$-\frac{1}{2}(1 + e)$	$-\frac{1}{2}(1 - e)$	$-\frac{1}{2}(3 - e)$	$\frac{1}{2}(1 + e)$
syn – conical jet	$\frac{1}{4}(5e - 3)$	$-\frac{1}{2}(3 - e)$	$-\frac{1}{2}(1 + e)$	$-(1 - e)$	$-\frac{1}{2}(3 - e)$	$\frac{1}{2}(1 + e)$
syn – spreading jet	$\frac{4}{3}e - 1$	$-\frac{2}{3}(3 - e)$	$-\frac{2}{3}e$	$-(1 - e)$	$-(2 - e)$	$e$
iC – spherical	$\frac{1}{4}(5e + 1)$	$-\frac{3}{4}(3 - e)$	$-\frac{1}{4}(5e + 1)$	$-1$	$-(2 - e)$	$2 + e$
iC – conical jet	$\frac{1}{2}(3e - 1)$	$-\frac{3}{4}(3 - e)$	$-\frac{1}{4}(5e + 1)$	$-\frac{1}{2}(3 - e)$	$-(2 - e)$	$2 + e$
iC – spreading jet	$\frac{4}{3}e$	$-(3 - e)$	$-\frac{5}{3}e - 1$	$-e$	$-(3 - 2e)$	$1 + 2e$

**Table 2.** Afterglow flux power-law decay index  $\alpha$  ( $F_\nu \propto t^{-\alpha}$ ) for the models listed in Table 1.  $p$  is the power-law index of the electron distribution with energy behind the forward-shock:  $dN/d\epsilon \propto \epsilon^{-p}$ , determined from the spectral slope  $\beta$ :  $p = 2\beta + 1$  for  $\nu_i < \nu < \nu_c$  and  $p = 2\beta$  for  $\nu_i, \nu_c < \nu$ .

MODEL	HOMOGENEOUS MEDIUM		WIND-LIKE MEDIUM	
	$\nu_i < \nu < \nu_c$	$\nu_i, \nu_c < \nu$	$\nu_i < \nu < \nu_c$	$\nu_i, \nu_c < \nu$
syn – spherical	$\frac{1}{4}(3p - 3) - \frac{1}{4}(p + 3)e$	$\frac{1}{4}(3p - 2) - \frac{1}{4}(p + 2)e$	$\frac{1}{4}(3p - 1) - \frac{1}{4}(p + 1)e$	$\frac{1}{4}(3p - 2) - \frac{1}{4}(p + 2)e$
syn – conical jet	$\frac{1}{4}3p - \frac{1}{4}(p + 4)e$	$\frac{1}{4}(3p + 1) - \frac{1}{4}(p + 3)e$	$\frac{1}{4}(3p + 1) - \frac{1}{4}(p + 3)e$	$\frac{1}{4}3p - \frac{1}{4}(p + 4)e$
syn – spreading jet	$p - \frac{1}{3}(p + 3)e$	$p - \frac{1}{3}(p + 2)e$	$p - \frac{1}{2}(p + 1)e$	$p - \frac{1}{2}(p + 2)e$
iC – spherical	$\frac{1}{8}(9p - 11) - \frac{1}{8}(3p + 7)e$	$\frac{1}{8}(9p - 10) - \frac{1}{8}(3p + 2)e$	$p - \frac{1}{2}(p - 1)e$	$p - 1 - \frac{1}{2}pe$
iC – conical jet	$\frac{1}{8}(9p - 5) - \frac{1}{8}(3p + 9)e$	$\frac{1}{8}(9p - 4) - \frac{1}{8}(3p + 4)e$	$p + \frac{1}{2} - \frac{1}{2}pe$	$p - \frac{1}{2} - \frac{1}{2}(p + 1)e$
iC – spreading jet	$\frac{1}{2}(3p - 3) - \frac{1}{6}(3p + 5)e$	$\frac{1}{2}(3p - 4) - \frac{1}{2}pe$	$\frac{1}{2}(3p - 3) - (p - 2)e$	$\frac{1}{2}(3p - 4) - (p - 1)e$

$$r \propto t^{\frac{e}{3-s}} \quad (24)$$

It is worth mentioning that the above dynamics of spreading jets undergoing energy injection can be recovered from the dynamics of a spreading adiabatic jet interacting with a homogeneous medium (equations 16, 17) if one replaces  $E \propto t^e$  (the prescription for energy injection) and  $r \propto \Gamma^2 t$ . The latter relation is trivial for an outflow decelerating as a power-law with radius (as for a spherical outflow or a conical jet) and is approximately satisfied for an exponential deceleration (as for an adiabatic spreading jet interacting with a homogeneous medium), which suggests that it should also stand in any other case of an intermediate-strength deceleration (that is verified with the numerical integration of the jet dynamics). Either from equations (22) and (24) or by replacing  $E$  and  $n \propto r^{-s}$  in equations (15) and (18) with the above prescriptions, it can be shown that

$$\Gamma \propto t^{-\frac{1}{2}(1 - \frac{e}{3-s})} \quad (25)$$

$$t' \propto t^{\frac{1}{2}(1 + \frac{e}{3-s})} (\propto r/\Gamma) \quad (26)$$

for a spreading jet and with energy injection.

By substituting equations (22)–(26) in the relations for the synchrotron and inverse-Compton spectral characteristics (equations 1–3 and 4–6), one can derive the evolutions from lines 3 and 6 of Table 1 and the power-law indices of the afterglow flux decay from lines 3 and 6 of Table 2.

We acknowledge that the dynamics of spreading jets undergoing energy injection was derived using a simplistic toy model for the jet lateral spreading, where the jet was assumed to have a uniform kinetic energy per solid angle  $dE/d\Omega$ , although both lateral spreading and energy injection could/should introduce a substantial angular gradient of  $dE/d\Omega$ , decreasing with angle measured from the jet’s spine.

## 3 ENERGY INJECTION IN SWIFT X-RAY AFTERGLOWS

### 3.1 Sample selection

Out of the 634 afterglow light-curves listed at the Swift-XRT light-curve repository (Evans et al 2007) posted until

**Table 3.** Light-curve breaks of well-sampled Swift X-ray afterglows. GRBs in bold-face have afterglow light-curve breaks that can be accounted for by an adiabatic jet-break (without energy injection). The GRBs listed in italics have a light-curve break that cannot be explained with a jet-break undergoing an energy injection continuous across the break

GRB	$\beta_x$	$t_{\text{start}}$ (ks)	$\alpha_{x1}$	$t_b$ (ks)	$\alpha_{x2}$	$t_{\text{end}}$ (Ms)	$E_\gamma$ (erg)	$z$
	(1)	(2)	(3)	(4)	(5)	(6)	(7)	(8)
050315	0.99(.09)	4	0.67(.03)	200	1.33(.16)	1		
<b>050401</b>	0.79(.13)	0.1	0.77(.12)	10	1.36(.08)	1	$4 \times 10^{53}$	2.90
050712	1.31(.14)	4	0.66(.10)	100	1.29(.18)	1.5		
050713B	1.08(.14)	4	0.56(.05)	70	1.20(.08)	1.5		
<b>050802</b>	0.86(.06)	0.4	0.71(.07)	10	1.66(.08)	1	$4 \times 10^{52}$	1.71
050803	1.12(.10)	0.5	0.40(.05)	10	1.75(.08)	1		
<b>050814</b>	0.97(.13)	2	0.82(.05)	100	1.89(.18)	1	$2 \times 10^{53}$	5.3
050822	1.11(.14)	7	0.46(.05)	70	1.09(.05)	4		
050922C	1.21(.11)	0.1	0.92(.10)	5	1.38(.10)	0.1	$1 \times 10^{53}$	2.20
<b>051016B</b>	0.89(.12)	4	0.75(.08)	40	1.25(.10)	0.7		
<b>051022</b>	1.07(.12)	10	1.44(.10)	200	2.19(.28)	1		
<b>051109</b>	1.06(.08)	4	1.12(.05)	70	1.31(.05)	2		
060105	1.05(.08)	0.1	0.84(.02)	2	2.25(.07)	0.03		
060111B	1.24(.17)	0.2	0.84(.07)	10	1.38(.16)	0.2		
060115	1.10(.12)	1	0.56(.15)	30	1.31(.17)	0.4	$8 \times 10^{52}$	3.53
<b>060204B</b>	1.21(.13)	5	1.17(.07)	40	1.76(.24)	0.3		
060210	1.08(.05)	4	0.99(.03)	100	1.43(.15)	1.5	$4 \times 10^{53}$	3.91
<i>060413</i>	0.90(.10)	5	0.08(.08)	30	2.79(.16)	0.2		
<b>060428</b>	0.94(.15)	1	0.63(.05)	100	1.19(.10)	1		
<i>060510</i>	0.88(.09)	0.2	0.05(.10)	5	1.44(.05)	0.4		
060604	1.17(.12)	2	0.50(.08)	30	1.22(.08)	1	$5 \times 10^{51}$	2.68
<i>060607</i>	0.61(.06)	0.6	0.40(.05)	20	3.16(.12)	0.1	$1.5 \times 10^{53}$	4.05
<i>060614</i>	0.90(.09)	3	0.04(.08)	40	2.17(.12)	2	$2 \times 10^{51}$	0.13
<i>060729</i>	1.02(.04)	0.6	0.08(.03)	100	1.36(.02)	3	$5 \times 10^{51}$	0.54
<b>060813</b>	0.92(.09)	0.2	0.99(.02)	40	2.06(.30)	0.2		
060814	1.12(.07)	1	0.34(.12)	6	1.01(.03)		$7 \times 10^{52}$	0.84
060814			1.01(.03)	70	1.74(.16)	0.6		
060908	1.13(.19)	0.2	0.81(.12)	1	1.34(.10)	0.4	$7 \times 10^{52}$	1.88
<i>061021</i>	0.99(.04)	4	0.92(.03)	100	1.16(.05)	4		
<i>061121</i>	0.90(.06)	0.3	0.02(.10)	10	1.56(.05)	2	$2 \times 10^{53}$	1.31
061222	0.93(.06)	0.3	0.36(.08)	10	1.06(.05)		$3 \times 10^{53}$	2.09
061222			1.06(.03)	100	1.70(.05)	1.5		
<b>070107</b>	1.08(.08)	6	1.00(.05)	100	1.84(.16)	0.8		
070129	1.28(.13)	1	0.19(.15)	20	1.21(.07)	2		
070220	0.56(.12)	0.6	0.76(.13)	3	1.14(.05)			
<b>070220</b>			1.14(.05)	20	2.01(.13)	0.1		
<i>070306</i>	0.94(.08)	0.7	0.05(.08)	30	1.88(.07)	1	$8 \times 10^{52}$	1.50
070328	1.14(.09)	0.15	0.38(.08)	0.8	1.12(.05)			
<b>070328</b>			1.12(.05)	5	1.58(.03)	1		
070420	0.97(.09)	0.3	0.27(.10)	3	1.21(.08)			
070420			1.21(.08)	50	1.83(.13)	0.5		
070508	0.82(.11)	0.4	0.99(.05)	2	1.48(.10)			
070508			1.48(.10)	60	1.67(.13)	0.6		
<b>070529</b>	0.98(.12)	0.2	0.76(.20)	2	1.31(.08)	0.4	$1.2 \times 10^{53}$	2.50
070628	1.04(.08)	1	0.37(.07)	7	1.19(.05)	0.08		
<b>071020</b>	0.61(.13)	0.1	1.23(.03)	80	1.64(.15)	1.5	$9 \times 10^{52}$	2.15
080319B	0.82(.06)	0.1	1.47(.02)	2	1.81(.02)	0.07	$1.3 \times 10^{54}$	0.94
<b>080319C</b>	0.61(.10)	0.4	0.84(.08)	4	1.53(.05)	0.3	$1.3 \times 10^{53}$	1.95
080320	0.97(.10)	1	0.66(.05)	80	1.19(.07)	2		
080328	0.95(.09)	0.3	0.62(.10)	3	1.21(.05)	0.04		
080413B	0.94(.06)	0.1	0.73(.03)	4	0.98(.05)		$2 \times 10^{52}$	1.10
<b>080413B</b>			0.98(.05)	70	1.49(.12)	0.6		
080430	1.04(.06)	0.6	0.45(.05)	50	1.12(.07)	3	$5 \times 10^{51}$	0.77
080703	0.49(.10)	0.1	0.58(.05)	20	2.01(.17)	0.1		
<b>080710</b>	1.01(.11)	3	1.05(.08)	30	1.71(.15)	0.3		
<b>080721</b>	0.91(.05)	0.1	0.82(.02)	2	1.65(.02)	1.4	$1.2 \times 10^{54}$	2.59
<b>080916</b>	0.89(.12)	0.3	0.68(.07)	40	1.24(.10)	1.4	$9 \times 10^{51}$	0.69
081007	1.10(.13)	0.5	0.77(.05)	40	1.24(.08)	1.5	$1.3 \times 10^{51}$	0.53
<b>081008</b>	0.99(.07)	0.6	0.88(.05)	20	1.82(.23)	0.3	$8 \times 10^{52}$	1.97
081028	1.04(.05)	20	1.30(.10)	80	2.30(.20)	0.5		
<i>081029</i>	0.96(.09)	3	0.45(.10)	20	2.18(.13)	0.1		

Table 3. (continued)

GRB	$\beta_x$	$t_{\text{start}}$ (ks)	$\alpha_{x1}$	$t_b$ (ks)	$\alpha_{x2}$	$t_{\text{end}}$ (Ms)	$E_\gamma$ (erg)	z
	(1)	(2)	(3)	(4)	(5)	(6)	(7)	(8)
<b>081203</b>	1.04(.09)	0.2	1.13(.03)	7	1.85(.08)	0.3	$3 \times 10^{53}$	2.05
081221	1.50(.12)	0.4	0.60(.08)	1	1.28(.05)			
081221			1.28(.05)	100	1.60(.23)	0.5		
081222	1.00(.06)	.08	0.85(.02)	2	1.18(.05)		$3 \times 10^{53}$	2.77
081222			1.18(.05)	70	1.83(.15)	0.7		
<b>090205</b>	1.02(.14)	1	0.77(.07)	20	1.84(.30)	0.2	$1.5 \times 10^{52}$	4.65
090401B	0.93(.10)	0.08	1.14(.02)	0.5	1.52(.05)	0.8		
090404	1.57(.13)	0.7	0.14(.08)	10	1.21(.03)	1		
090407	1.34(.12)	10	0.61(.07)	100	1.84(.18)	1		
090418	1.03(.09)	0.2	0.28(.18)	3	1.58(.05)	0.3	$1.6 \times 10^{53}$	1.61
<i>090424</i>	0.95(.09)	2	1.20(.05)	300	1.44(.08)			
090424			0.87(.02)	2	1.20(.05)	0.3	$4 \times 10^{52}$	0.54
090510	0.76(.12)	0.1	0.74(.05)	1.5	2.20(.16)	0.06	$2 \times 10^{52}$	0.90
090516	1.08(.07)	4	0.88(.10)	20	1.75(.07)	0.5		
090618	0.92(.05)	0.5	0.61(.03)	5	1.44(.02)		$2 \times 10^{53}$	0.54
090618			1.44(.02)	300	1.83(.13)	3		
090813	0.89(.09)	0.1	0.18(.10)	0.5	1.29(.02)	0.7		
091018	0.98(.08)	0.06	0.41(.07)	0.7	1.20(.05)		$5 \times 10^{51}$	0.97
091018			1.20(.05)	40	1.61(.13)	0.5		
091020	1.09(.06)	0.2	0.80(.10)	10	1.37(.03)	1	$8 \times 10^{52}$	1.71
091029	1.12(.07)	0.8	-0.23(.20)	4	0.86(.07)		$8 \times 10^{52}$	2.75
091029			0.86(.07)	100	1.23(.12)	2		
091127	0.80(.11)	3	1.20(.02)	100	1.60(.07)	4		
091130B	1.37(.14)	3	0.34(.07)	50	1.14(.07)	2		
<b>091208B</b>	1.04(.13)	5	1.10(.07)	100	1.57(.24)	1		
<b>100302</b>	0.94(.11)	5	0.66(.17)	50	0.92(.13)	1	$3 \times 10^{52}$	4.81
<i>100508</i>	0.43(.11)	1	0.39(.07)	20	2.32(.15)	0.2		
100522	1.28(.13)	0.2	0.45(.12)	3	0.84(.08)			
100522			0.84(.08)	40	1.37(.15)	0.4		
100619	1.29(.12)	0.3	0.86(.03)	30	1.22(.13)	0.8		
100621	1.31(.11)	0.5	0.56(.08)	7	0.99(.05)		$4 \times 10^{52}$	0.54
100621			0.99(.05)	100	1.61(.12)	2		
100704	1.12(.10)	0.6	0.98(.02)	300	1.84(.18)	1		
100728	0.90(.07)	1	1.21(.01)	30	1.54(.08)	0.6		
<i>100814</i>	0.89(.04)	4	0.52(.03)	100	1.94(.07)	2	$1.6 \times 10^{53}$	1.44
100906	1.04(.08)	0.3	0.53(.16)	6	1.69(.07)		$2 \times 10^{53}$	1.73
<b>100906</b>			1.69(.07)	60	2.21(.18)	0.3		
<b>101023</b>	1.14(.10)	3	1.10(.07)	30	1.43(.10)	0.6		
<i>101024</i>	0.82(.12)	0.1	0.00(.16)	1	1.37(.07)	0.1		
101117B	1.17(.16)	0.06	0.73(.08)	2	1.17(.10)	0.1		
110102	1.13(.06)	0.5	0.31(.25)	5	1.38(.05)			
<b>110102</b>			1.38(.05)	100	2.05(.26)	1		
<b>110213</b>	0.96(.06)	1	0.97(.07)	10	1.99(.08)	0.6		
110223B	0.73(.15)	0.1	0.86(.05)	5	1.16(.08)	0.4		
110420	1.05(.08)	0.2	0.23(.08)	3	1.18(.03)			
<b>110420</b>			1.18(.03)	200	2.09(.25)	2		
110422	0.89(.07)	0.8	1.01(.03)	8	1.52(.03)	0.7		
<i>110503</i>	0.91(.05)	0.2	1.06(.02)	20	1.39(.05)	0.8	$1.7 \times 10^{53}$	1.61
110709	1.06(.11)	0.2	0.78(.03)	7	1.70(.07)	0.3		
110709B	1.13(.06)	2	1.01(.03)	100	1.57(.07)	1		
<b>110715</b>	0.86(.10)	0.08	0.57(.05)	1	1.52(.10)	0.03	$4 \times 10^{52}$	0.82
110731	0.85(.10)	0.08	1.16(.03)	30	1.29(.10)	0.8	$4 \times 10^{53}$	2.83
110915	1.25(.14)	0.3	0.88(.05)	10	1.44(.05)	0.4		
111008	0.96(.07)	0.3	0.07(.18)	3	1.12(.07)		$4 \times 10^{53}$	4.99
111008			1.12(.07)	50	1.54(.12)	0.5		
111228	1.05(.07)	0.5	0.25(.07)	10	1.13(.03)	1	$3 \times 10^{52}$	0.71

(1): X-ray spectral slope (90 percent CL)

(2): epoch of first Swift X-ray measurement

(3): index of X-ray flux power-law decay at  $t_{\text{start}} - t_b$  (90 percent CL)

(4): epoch of X-ray light-curve break

(5): index of X-ray flux power-law decay at  $t_b - t_{\text{end}}$  (90 percent CL)

the end of year 2011, we have retained only those for which *i*) a light-curve break is obvious or seems possible, *ii*) a power-law light-curve segment is monitored for longer than a factor 5 in time before and after the break, and *iii*) the spectral slope  $\beta_x$  listed at the Swift-XRT spectra repository (Evans et al 2007) has a 90 percent confidence level (CL) less than 0.16.

The light-curves have been piece-wise fit with power-laws, using measurements sufficiently far from the break time, to capture the asymptotic power-law flux decay. Shallow breaks for which the data could be fit satisfactorily (i.e. reduced  $\chi^2_v \simeq 1$ ) with a single power-law were excluded. The 90 percent confidence level ( $\sigma(\alpha_x)$ ) was determined from the variation of  $\chi^2$  around the best power-law fit.

As shown in Table 2, for an adiabatic outflow ( $e = 0$ ), the power-law index is  $\alpha_x = 3p/4 + \text{const} = 3\beta_x/2 + \text{const}$ , with the coefficient of  $\beta_x$  being as large as 9/8 for other models. Thus, an equal importance of measurement uncertainties  $\sigma(\alpha_x)$  and  $\sigma(\beta_x) \leq 0.16$  requires that we retain only afterglows whose decay indices can be determined with a 90 percent CL smaller than  $1.5\sigma(\beta_x) \simeq 0.24$ .

The above two basic selection criteria led to the sample of 98 afterglows and 117 X-ray light-curve breaks listed in Table 3. Forty-four afterglows have temporal coverage starting from the burst end (for them, we determine the fractional increase of the outflow energy during the afterglow phase) and a measured redshift, which allows the calculation of the GRB output and of the afterglow jet energy.

The light-curves of the afterglows listed in Table 3 are morphologically diverse. A minority display a continuous, slowly-decaying power-law flux from the burst phase to the afterglow, the afterglow beginning being chosen when the flux fluctuations disappear. The majority of GRBs display a sharp decay after the prompt phase (the GRB tail) followed by a much slower decay and spectral hardening; the afterglow beginning is chosen at the epoch when the slower flux decay starts.

The closure relations  $\alpha - \beta$  listed in Table 2 are used to calculate the required energy injection indices from the measured pre- and post-break X-ray flux decay indices  $\alpha$  and the X-ray slope  $\beta$  (which gives the electron index  $p$ ). For a model to be validated, the resulting energy injection index  $e$  *i*) should be positive (i.e.  $e + \sigma_e > 0$ , with the uncertainty  $\sigma_e$  calculated from the propagation of  $\sigma(\alpha_x)$  and  $\sigma(\beta_x)$ ), and *ii*) for jet-break models, should lead to a decelerating outflow, so that the jet boundary can become visible to the observer at some time. From equation 11, this condition is  $e < 3 - s$ .

### 3.2 Adiabatic jets

For adiabatic jets ( $e = 0$ ), the observables  $\alpha_{x1}$  and  $\alpha_{x2}$  yield two constraints. As there are no free model parameters, aside the various possibilities related to the jet dynamics, location of the cooling frequency, ambient medium type, and dominant X-ray emission process, the model is over-constrained. Thus, it should not be surprising that only a small fraction of Swift X-ray breaks satisfy  $|e| < \sigma_e$  both before and after the break, i.e. can be explained by any single variant of the adiabatic jet break model (upper part of Table 4).

**Table 4.** Number of breaks that can be accommodated by an adiabatic jet-break, a jet-break with steady energy injection, or by an energy-injection break, out of the 117 breaks listed in Table 3. Models are identified by the origin of the X-ray light-curve break (“J” = jet-break, “EI” = energy-injection break), radiation process dominant in the X-rays (“syn” = synchrotron, “iC” = inverse-Compton) and by the jet dynamics (“cjet” = conical jet, “sjet” = spreading jet, “sph” = spherical – see Table 2).

MODEL	HOMOG MEDIUM		WIND-LIKE MEDIUM	
	$\nu < \nu_c$	$\nu_c < \nu$	$\nu < \nu_c$	$\nu_c < \nu$
<b>adiabatic jet-break</b>				
J-syn-cjet	3	11	0	9
J-syn-sjet	0	7	0	7
J-iC-cjet	2	15	0	9
J-iC-sjet	2	7	0	7
<b>jet-break with or without steady EI</b>				
J-syn-cjet	48	47	12	29
J-syn-sjet	19	39	15	42
J-iC-cjet	64	52	0	31
J-iC-sjet	67	18	0	16
<b>energy-injection break</b>				
EI-syn-cjet	111	98	113	77
EI-syn-sjet	115	106	115	105
EI-syn-sph	77	31	106	31
EI-iC-cjet	114	4	116	80
EI-iC-sjet	114	47	114	54
EI-iC-sph	105	37	115	36

Evidently, Swift X-ray afterglows may not be all of the same forward-shock model type. Even when we take into account all these possible variants, we find that adiabatic jet-break model can explain only 30 afterglows (indicated in boldface in Table 3), i.e. about 30 percent of the sample considered here. Six of those 30 breaks occur in afterglows with two light-curve breaks, the break compatible with an adiabatic jet-break being always the second. For all six, there is always a spherical energy-injection break model with  $e = 0$  after the break that accounts for the first break, and compatible with the jet-break model, i.e. the two break models have the same location of cooling frequency relative to the X-rays, the same type of external medium, and the same X-ray emission process.

### 3.3 Energized jets

#### 3.3.1 Jet-breaks

For the jet-break model, we require that the X-ray light-curve break arises solely from the outflow collimation, without any contribution from a break in the injected power, i.e. we require a constant energy injection index  $e$  across the X-ray light-curve break:  $(e_1 - e_2)^2 < \sigma_{e_1}^2 + \sigma_{e_2}^2$ . Thus, the model is still over-constrained, with two observables ( $\alpha_{x1}$  and  $\alpha_{x2}$ ) that must be accommodated by a single model parameter ( $e$ ). Considering that the jet-break model with steady energy injection is less over-constrained than the adiabatic jet model, it may not be surprising that the former model



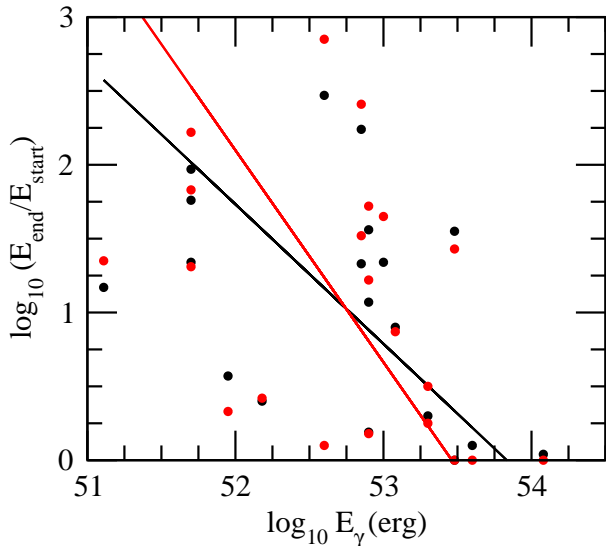


**Figure 1.** Fractional increase of the jet energy from (source frame) 100 s to 100 ks ( $E_{\text{end}}/E_{\text{start}}$ ) versus GRB output at 10 keV – 10 MeV ( $E_{\gamma}$ ) and whose X-ray light-curve breaks can be accommodated by a conical jet-break with steady energy injection (other model details: X-ray higher than the synchrotron cooling frequency, external medium is homogeneous). Black points are for a model where synchrotron is the dominant X-ray radiative process, red points for an inverse-Compton model. These are the afterglows listed in Table 3 for which a redshift is known and whose light-curve breaks (first break, if two exist) can be accommodated by the models described above. In natural scale,  $E_{\text{end}}/E_{\text{start}}$  and  $E_{\text{end}}/E_{\text{start}}$  are uncertain by up to 50 percent, hence their logarithms are uncertain by up to 0.20 .

can account for a larger number of Swift breaks (mid part of Table 4).

With allowance for all jet-break model variants listed in Table 4 (i.e. for either location of the cooling frequency relative to the X-ray, for either radiation process, for either type of medium, and either post jet-break dynamics, conical or spreading), the jet-break model with steady energy injection (including adiabatic jet-breaks, for which the energy injection parameter  $e$  is consistent with zero) can account for 103 of the 117 X-ray light-curve breaks considered here (the unexplained breaks are shown in italics in Tables 3). 37 of those potential jet-breaks occur in afterglows with two light-curve breaks; with the exception of the first break of afterglow 081222, all other 36 jet-breaks can be paired consistently with an energy-injection break for the remaining break, i.e. the two break models have the same medium stratification, the same X-ray radiative process, the same location of X-ray relative to the cooling frequency, and compatible ejecta dynamics.

Because only one break can arise from the outflow collimation and 19 afterglows in our sample have two light-curve breaks, a more correct way of assessing the success of the jet-break model with steady energy injection is to say that it can explain at least one of the breaks observed for 85 afterglows out of 98 or, conversely, that it cannot account for any of the X-ray light-curve breaks of 12 percent of afterglows. Excluding the 30 breaks (of 30 afterglows) that can be accounted for with an adiabatic jet-break, the jet-break

model with non-zero energy injection can explain one X-ray light-curve break for 55 of the 98 afterglows considered here, which argues strongly that energy injection may be often present in Swift afterglows.

### 3.3.2 Energy injection breaks

Given that 12 percent of afterglows have an X-ray light-curve break that cannot be explained with a jet-break even when a steady energy injection is allowed, and that some afterglows display two breaks, out of which only one can be a jet-break, it is natural to speculate that some X-ray light-curve breaks must arise from a change in the power at which energy is added to the forward-shock. In the extreme, one could speculate that all X-ray breaks could be such energy injection breaks, but the large fraction of breaks that can be explained as jet-breaks argues against that extreme speculation.

The broken power-law energy injection model is not over-constrained, as there are two observables ( $\alpha_{x1}$  and  $\alpha_{x2}$ ) for two model parameters ( $e_1$  and  $e_2$ ), the only restriction being that  $e > 0$ . Thus, it should not be surprising that there are variants of the energy-injection break model that can account for most of the Swift X-ray breaks (lower part of Table 4). There is only one X-ray break that cannot be explained with an energy injection break: GRB afterglow 060607. From Table 2, it can be seen that, for  $\beta_x < 3/2$ , the steepest possible decay for an adiabatic outflow is that for the inverse-Compton emission from a conical jet interacting with a wind, and for  $\nu_x < \nu_c$ :  $\alpha_x = p + 1/2 = 2\beta_x + 3/2$ \*. For GRB afterglow 060607,  $\beta_x = 0.61 \pm 0.06$ , hence the steepest possible decay for the forward-shock emission has  $\alpha_x = 2.72 \pm 0.12$ , which is slower than the measured post-break  $\alpha_{x2} = 3.16 \pm 0.07$ .

## 4 IMPLICATIONS OF ENERGY INJECTION

### 4.1 Afterglow decay rate – GRB output correlation

After having identified the power-law energy injection that accommodates each of the X-ray light-curve breaks, one can calculate the increase in the forward-shock energy from first to last X-ray measurement. The interesting result is that the fractional increase of the forward-shock energy over a source-frame time-interval common to all afterglows (from 100 s to 100 ks),  $f_{\text{ag}} \equiv E_{\text{end}}/E_{\text{start}}$ , is anticorrelated with the isotropic-equivalent GRB output  $E_{\gamma}$ , for any model variant that can account for a significant fraction of the afterglow breaks listed in Table 3.

The  $E_{\gamma} - f_{\text{ag}}$  anticorrelation is illustrated in Figure 1

\* For  $\beta_x > 1/2$ , the fastest decay  $\alpha_x = 2\beta_x + 3/2$ , exceeds the  $\alpha_x = \beta_x + 2$  limit for the large-angle emission decay, resulting when the emission from a spherical outflow stops suddenly; however, for a jet seen after the jet-break time, the large-angle emission does not exist because there is no radiating fluid at angles larger than  $\Gamma^{-1}$

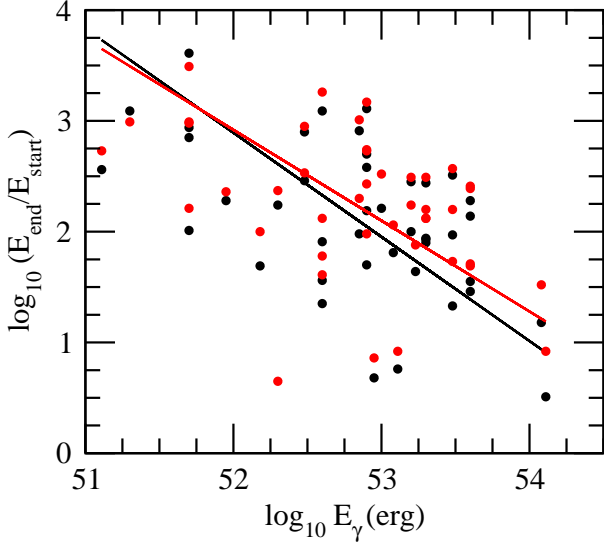


**Figure 2.** Similar to Fig 1, but for energy-injection break as the origin of the X-ray light-curve break, with the afterglow outflow being a conical jet and the jet-break having occurred at early times (before the first X-ray measurement). The ambient medium is homogeneous and X-ray assumed to be below the cooling frequency. Black points are for synchrotron as the dominant X-ray process, red points are for an inverse-Compton model.

for two jet-break models and in Figure 2 for two energy-injection break models. For the synchrotron jet-break model (black points in Figure 1), the linear correlation coefficient in log-log space is  $r = -0.42 \pm 0.08$ , yielding a probability for a stronger anticorrelation  $prob < 0.080$  in the null hypothesis. For the inverse-Compton jet-break model (red points in Figure 1),  $r = -0.40 \pm 0.07$  and  $prob < 0.076$ . For the synchrotron energy-injection break model (black points in Figure 2),  $r = -0.54 \pm 0.04$ , and  $prob < 0.52 \times 10^{-3}$ , while for the inverse-Compton energy-injection break model (red points in Figure 2),  $r = -0.43 \pm 0.06$ , and  $prob < 0.70 \times 10^{-2}$ . Similarly high chance probabilities are obtained for other models; thus the  $E_\gamma - f_{ag}$  anticorrelation is only “tentative”.

The above linear correlation coefficients (Pearson’s  $r$ ) have been calculated assuming a 50 percent uncertainty (in natural scale) for both quantities plotted, the chance probabilities of those anticorrelations have been estimated conservatively for a linear correlation coefficient  $|r| - \sigma(r)$ . The best-fits shown in Figures 1 and 2 were obtained by minimizing  $\chi^2$  using the uncertainties of both quantities.

That *i*) the fractional increase of the forward-shock energy over a fixed time interval is determined by the exponent  $e$  of the power-law energy injection which accommodates the measured X-ray flux decay index  $\alpha_x$ , and that *ii*)  $d\alpha/de < 0$  (a stronger energy injection yields a slower flux decay) suggest that the  $E_\gamma - f_{ag}$  correlation may originate from a  $\log E_\gamma - \alpha_x$  correlation. Indeed, as illustrated in Figure 3, more energetic bursts are followed by faster decaying X-ray afterglows. The correlation between these two observables is slightly stronger than the  $E_\gamma - f_{ag}$  correlation for afterglows with jet-breaks at the X-ray light-curve epoch, but significantly weaker if the X-ray light-curve breaks are energy-injection breaks.

The  $E_\gamma - f_{ag}$  correlation implies that either the efficiency of the GRB mechanism or the energy of the ejecta producing the GRB emission are anticorrelated with the kinetic energy of the ejecta interacting with the forward-shock after the burst phase.

If the dissipation mechanism leading to the production of  $\gamma$ -rays is internal shocks (Rees & Meszaros 1994) in a fluctuating relativistic wind, then the burst dissipation efficiency is determined by the ratio between the Lorentz factors of interacting shells. For an *impulsive* ejecta release (short-lived engine), all the ejecta are produced quasi-instantaneously and the energy injection occurs as the inner parts of the outflow catch-up with the ever-decelerating forward-shock (Rees & Meszaros 1998). In this model, the  $E_\gamma - f_{ag}$  correlation implies an anticorrelation between the average shells’ Lorentz factor ratio with the energy of the shells behind the leading edge of the outflow, smoother outflows (i.e. with a smaller Lorentz factor contrast) having more energy localized toward the trailing edge. For an *extended* ejecta release (long-lived engine), where the ejecta are released over a source-frame duration comparable to the observer-frame time during which energy injection takes place, the  $E_\gamma - f_{ag}$  correlation would imply an anticorrelation among bursts between the Lorentz factor contrast in the leading, GRB-producing part of the outflow and the kinetic energy of the outflow expelled by the central engine at later times. This is a puzzling implication, which makes the long-lived engine scenario less likely.

Irrespective of the dissipation mechanism, if the GRB output is correlated with the energy of the GRB-producing ejecta, then the  $E_\gamma - f_{ag}$  correlation implies a relationship between the GRB ejecta energy and the radial distribution of the afterglow outflow energy. For a short-lived central engine, where the GRB and afterglow outflows are the same, the  $E_\gamma - f_{ag}$  correlation would require that more energetic outflows have less energy behind the leading front. For a long-lived central engine, where the GRB outflow is the early afterglow blast-wave, the  $E_\gamma - f_{ag}$  correlation implies that engines that are initially more energetic release less energy after the burst. Perhaps this scenario appears more plausible because it opens the possibility of a constant total ejecta energy. Unfortunately, we do not find that  $f_{ag} E_\gamma$  is universal; instead, its distribution extends over at least two decades, for the  $f_{ag}$  calculated in any light-curve break model.

We note that the detection of X-ray flares in some Swift afterglows indicates an extended ejecta release, but the energetic output of those flares is only about 10 percent of the prompt GRB output (Falcone et al 2007). In contrast, the energy injection required during the afterglow phase corresponds to an increase of the outflow energy after the burst by a factor up to  $10^4$  (Figures 1 and 2). To reconcile the flare and afterglow energetics, the internal shocks that produce flares must be very inefficient X-ray radiators compared to the forward-shock (see also Maxham & Zhang 2009) or, else, the X-ray flares could be produced by the central engine, bearing little correlation with the energy of the ejecta released after the burst.

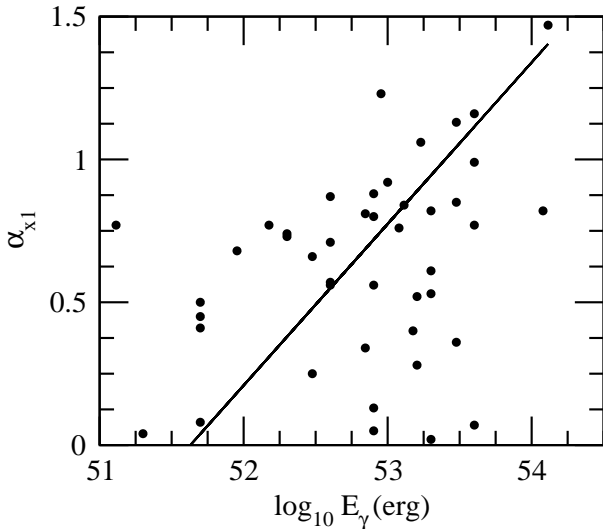


**Figure 3.** Correlation of power-law index  $\alpha_{x1}$  of the early afterglow X-ray flux decay and GRB output  $E_\gamma$  for 44 Swift afterglows. Linear correlation coefficient is  $r = 0.34 \pm 0.05$ , with a chance probability  $prob < 0.026$ .

## 4.2 Afterglow energetics

The large increase of the forward-shock energy, by a factor  $f_{ag} = 10 - 300$  (Fig 1) or  $f_{ag} = 10 - 10^4$  (Fig 2), required to account for the light-curve breaks of Swift X-ray afterglows raises the question if the total outflow energy is not too large and incompatible with the expected energy reservoir for a few solar-masses black-hole and its sub solar-mass torus formed in the collapse of a WR massive star.

The jet energy can be estimated by assuming that, at the first X-ray measurement ( $t_{start}$ ), the isotropic-equivalent forward-shock energy is the GRB output  $E_\gamma$ . This assumption introduces an underestimation of the jet energy by a factor up to a few because energy could be injected into the forward-shock even before  $t_{start}$  (100 - 1000 s), maybe starting as early as the burst end (10 - 100 s), at a rate  $E \propto t^{1/3} - t^1$  (this is the range of energy injection laws that accommodate the early X-ray flux decays of Table 3), and with the estimated jet energy satisfying  $E_j \propto [E(t_{start})]^{3/4}$  for a homogeneous medium and  $E_j \propto [E(t_{start})]^{1/2}$  for a wind. For a short-lived engine, where all the outflow produces the burst emission and only its leading edge yields the early afterglow, we have  $E(t_{start}) \ll E_\gamma$ ; in this case, the total jet energies calculated here may be substantially overestimated. For a long-lived engine, where the leading part of the outflow produces both the burst and early afterglow emissions,  $E(t_{start}) = E_\gamma$  is equivalent to assuming a (reasonable) 50 percent GRB efficiency.

The jet initial aperture  $\theta_j$ , needed to calculate the jet energy from isotropic equivalents, can be constrained as following. For the model of a narrow jet whose edge becomes visible before the first X-ray measurement and the X-ray light-curve break is an energy injection,  $\theta_j < 1/\Gamma(t_{start})$ . For the model where the X-ray light-curve break (at  $t_b$ ) is a jet-break undergoing a steady energy injection,  $\theta_j = 1/\Gamma(t_b)$ . For the model of a wide jet whose edge becomes visible after the last X-ray measurement ( $t_{end}$ ),  $\theta_j > 1/\Gamma(t_{end})$ . Prior

to the jet-break, the jet Lorentz factor is given by the dynamics of a spherical blast-wave:

$$\Gamma(t) = 800 \left[ \frac{E_{53}(t)}{n_o} \right]^{1/8} \left( \frac{t}{z+1} \right)^{-3/8} \quad (27)$$

for a homogeneous medium of particle density  $n_o$  per  $\text{cm}^{-3}$  and

$$\Gamma(t) = 175 \left[ \frac{E_{53}(t)}{A_*} \right]^{1/4} \left( \frac{t}{z+1} \right)^{-1/4} \quad (28)$$

for a wind-like medium of density  $n \propto Ar^{-2}$  normalized to that corresponding to progenitor mass-loss rate-to-terminal speed ratio of  $(dM/dt)/v = 10^{-5} (M_\odot \text{ yr}^{-1}) / (10^3 \text{ km s}^{-1})$ , respectively, with  $E_{53}(t) = 10^{-53} E(t)$  being the blast-wave isotropic-equivalent energy at observer time  $t$ . The latter is calculated assuming that  $E(t_{start}) = E_\gamma$  and for the energy injection law  $E \propto t^e$  required for each model to account for the measured X-ray flux decay. The observer time in the above equations corresponds to the arrival-time of photons emitted by the fluid moving at an angle  $\theta = \Gamma^{-1}$  relative to the direction toward the observer, from where arises most of the high-energy emission received by the observer at time  $t$ .

Putting together all the elements described above, we have calculated the jet final energy (at  $t_{end}$ ) for the X-ray afterglows whose light-curve breaks can be explained by the a jet-break model with steady energy injection or an energy-injection break model (the models listed in the mid and lower parts of Table 4). The jet energies for  $n_o = 1$  and  $A_* = 1$ , averaged over all the afterglows that can be accounted for by each model (fewer than indicated in Table 4, because the jet energy calculation requires the GRB output/burst redshift), are listed in Table 5. For jet-breaks models, the jet opening is determined by the light-curve break epoch. For energy injection-break models, the epoch of the first (last) X-ray measurement provide an upper (lower) limit on the jet-break epoch, which yields an upper (lower) limit on the jet opening and, consequently, on the jet energy. Numbers in round brackets give the dispersion of individual jet energies (or their lower/upper limits).

A potentially important result shown in Table 5 is that models where X-ray is inverse-Compton, the ambient medium is a wind, and X-ray is lower than the cooling frequency, can be ruled out on energetic grounds because, for them, the required jet total energy exceeds  $10^{53.5} \text{ erg}^\dagger$ . Those models lead to a high final jet energy because a substantial increase of the jet energy is required to account for the measured X-ray flux decay rate, which stems from that the corresponding adiabatic jet model yields a steep X-ray flux decay (Table 2:  $\alpha_x = p + 1/2 = 2\beta_x + 3/2$ , for a conical

<sup>†</sup> Magneto-hydrodynamic simulations of accretion disks (e.g. McKinney 2005, Hawley & Krolik 2006) show that the energy in relativistic matter (electromagnetic outflow) extracted from an accreting black-hole increases from 0.2 (0.03) percent of the accreted mass, for a non-rotating black-hole, to 15-40 (5-20) percent for a maximally rotating one. The maximal energy budget quoted here corresponds to a 20 percent MHD efficiency and a  $1 M_\odot$  accretion disk.

**Table 5.** Average (and dispersion) of the logarithm of jet energy (in ergs) at the last X-ray measurement, for the models in the two lower sections of Table 4.

MODEL	HOMOG MEDIUM		WIND-LIKE MEDIUM	
	$\nu < \nu_c$	$\nu_c < \nu$	$\nu < \nu_c$	$\nu_c < \nu$
jet-break				
J-syn-cjet	50.4(0.5)	49.9(0.6)	51.1(0.6)	49.9(0.3)
J-syn-sjet	50.3(0.8)	50.1(0.7)	51.5(0.6)	50.2(0.4)
J-iC-cjet	50.7(0.6)	49.8(0.7)	—	50.0(0.3)
J-iC-sjet	50.6(0.7)	49.6(0.6)	—	49.7(0.3)
energy-injection break				
EI-syn-cjet <	50.0(0.6)	49.7(0.6)	51.7(0.7)	49.9(0.5)
EI-syn-sjet <	50.8(0.7)	50.2(0.7)	51.7(0.6)	50.3(0.4)
EI-syn-sph >	51.0(0.5)	50.6(0.4)	51.8(0.6)	50.6(0.3)
EI-iC-cjet <	50.2(0.7)	49.7(0.7)	53.6(0.8)	50.0(0.5)
EI-iC-sjet <	50.4(0.8)	48.9(0.8)	55.0(1.3)	49.5(0.6)
EI-iC-sph >	51.4(0.6)	50.7(0.5)	53.3(0.8)	50.6(0.3)

jet), from that energy injection has a weak effect in mitigating the flux decay ( $d\alpha_x/de = p - 2 = 2\beta_x - 1$ , for the spreading jet model), or a combination of those two factors (for the spherical outflow model).

Assuming the same jet energy at the beginning of the afterglow, one can also calculate the ratios of jet energies among the three types of X-ray break models and outflow dynamics: *i*) a narrow-jet model with an energy-injection break (models E-cjet and E-sjet in Table 5), *ii*) a jet-break model with steady energy injection (models J-cjet and J-sjet), and *iii*) a wide-jet model with energy-injection break (model E-sph). The interesting result is that, going from type *i*) to type *ii*) models above increases on average (i.e over afterglows) the total jet energy by a factor 2-3, with another increase by a factor 2-3 required when going from type *ii*) to *iii*) models. These results hold for either type of ambient medium, either location of the cooling frequency relative to the X-ray, and for either X-ray radiative process, if the jet does not spread sideways, and only for inverse-Compton emission, if the jet is spreading laterally. Thus, the most economical model for a light-curve break is that of a narrow jet with an early jet-break and a broken power-law energy injection origin for the X-ray light-curve break. However, these conclusions do not hold for spreading jets if the X-ray radiation process is synchrotron. In this case, we find that the required jet energy is about the same for all model types above. Note that these relative energy requirements cannot be deduced from the average jet energies listed in Table 5. Here, we are referring to averages over afterglows of jet energy ratios between two models that explain the same afterglow break, while Table 5 gives jet energies for a given model averaged over all the afterglows that can be explained by that model.

### 4.3 Loose ends

The first caveat/weakness of the model testing presented above was already discussed: the energy-injection break origin for X-ray light-curve breaks is only weakly falsifiable

by a comparison between the model  $\alpha - \beta$  closure relation and the observed flux power-law decay index  $\alpha$  and spectral slope  $\beta$ . The only way for this model to fail is an X-ray flux that decays steeper than expected for an adiabatic shock, as energy injection can only mitigate the afterglow flux decay.

Furthermore, a comparison of the model light-curve breaks against observations is needed to validate possible X-ray light-curve break models, as the sharpness of X-ray light-curve breaks varies among afterglows. The majority of the well-sampled light-curve breaks used here are sharp, lasting less than a factor two in time. Quite likely, the sharpest breaks cannot be accounted by a wind-like medium, whatever is the break mechanism, owing to the slower jet deceleration produced by a decreasing external density (Kumar & Panaitescu 2000). Without taking into account such limitations, testing only the ability of some models to account for the observed flux power-law decay indices will overestimate the fraction of afterglows that can be explained by a given model.

We emphasize the importance of using afterglows whose light-curves have been sampled over a sufficiently long time before and after the break, so that the asymptotic flux decay indices can be measured accurately. Otherwise, shortly-monitored light-curves with breaks can lead to an underestimation of the break magnitude  $\delta\alpha = \alpha_{x2} - \alpha_{x1}$ , which will favour a steady energy injection interpretation, because its effect is to reduce the break magnitude  $\delta\alpha$ . We note that eighty percent of the power-law segments used in this work last a decade or more in time.

#### 4.3.1 Optical afterglows

Inclusion of the optical light-curves could provide a further test to the origin of X-ray light-curve breaks (e.g. Liang et al 2007; Curran et al 2009; Liang et al 2008) in the two models discussed above (jet-break and energy-injection break). Both models yield *achromatic* light-curve breaks, appearing at the same time in all light-curves. For those afterglows where it can be established that the optical and X-ray emissions arise from the same source, either because the light-curve breaks are achromatic or because the optical and X-ray spectra are on the same power-law continuum, testing the light-curve break origin and determining the model details (location of cooling frequency, ambient medium stratification, radiation process, outflow dynamics) can be done by comparing the optical flux decay indices  $\alpha_o$  with the model expectations, for the energy injection parameter  $e$  required by the X-ray flux decay indices  $\alpha_x$ .

In GRBlog database of optical light-curves (Quimby, McMahon & Jeremy 2004), we find five afterglows (050401, 061121, 070420, 090424, 090618) listed in Table 3 with chromatic X-ray breaks, hence their X-ray and optical emissions arise from different parts of the outflow, and eight with achromatic breaks, thus a comprehensive test of the X-ray break models cannot be performed at this time. We note that, of those 8 afterglows with achromatic breaks, two (060729, 081029) have  $\alpha_x \simeq \alpha_o$ , for five (050922C, 051109, 060614, 080710, 090424)  $0.25 < \alpha_x - \alpha_o < 0.5$ , and for one (090510)  $\alpha_x - \alpha_o \simeq 1$ .

In general,  $\alpha_x = \alpha_o$  (as for 060729) is expected if the

cooling frequency is not between the optical and X-ray and  $\alpha_x - \alpha_o = -(1/2)d \log \nu_c / d \log t$  if  $\nu_c$  is in between. According to Table 1, a decreasing  $\nu_c$  (which leads to  $\alpha_x > \alpha_o$ ), is obtained only for a homogeneous medium, thus all six afterglows with  $\alpha_x - \alpha_o \geq 0.25$  require such an ambient medium. Energy injection accelerates the evolution of  $\nu_c$  and increases the index difference  $\alpha_x - \alpha_o$  above the expectation for an adiabatic outflow:  $\alpha_x - \alpha_o = (e + 1)/4$  for a spherical/conical outflow and  $\alpha_x - \alpha_o = e/3$  for a spreading jet. Thus, the energy injection indices  $e$  in the range (0.3, 1) required by the X-ray decays of those six afterglows imply that  $0.3 < \alpha_x - \alpha_o < 0.5$ , consistent with what is measured for five of them, while the large  $\alpha_x - \alpha_o$  measured for 090510 indicates that the optical and X-ray are from different radiative processes (synchrotron and inverse-Compton, respectively).

#### 4.3.2 Reverse shock

In this work, we have considered only the forward-shock emission and ignored the emission from the reverse-shock, which energizes the GRB/post-GRB ejecta, the agent of energy injection into the blast-wave. The two shocks dissipate equally the kinetic energy of the ejecta, which indicates that the reverse-shock could make a comparable contribution to the afterglow emission.

For a short-lived ejecta source, it can be shown from the kinematics of the catch-up between the GRB ejecta and the decelerating forward-shock that the ratio of the Lorentz factor  $\Gamma_i$  of the ejecta arriving at the forward-shock at time  $t$  to that of the swept-up ambient medium  $\Gamma(t)$  is  $\Gamma_i/\Gamma(t) = [(4 - s)/(1 + e)]^{1/2} \gtrsim 1$  (evidently, the ratio of those two Lorentz factors must be above unity, but cannot be much above unity, else the catch-up would have occurred earlier). In this case, the reverse shock is only mildly relativistic and the ejecta electrons accelerated by the reverse-shock could be much less energetic than the electrons behind the forward-shock, making the emission of the latter dominant at X-ray photon energies.

For a long-lived central source, the contrast between the Lorentz factor of the unshocked outflow and that of the forward-shock can be arbitrarily large, the reverse-shock could be highly relativistic, provided that the ejecta are not too dense (e.g. Sari & Piran 1995). The decay of the reverse-shock flux can be calculated in a way similar to that shown here for the forward-shock; however, the parametrization of the reverse-shock emission is not that simple because *i*) its dynamics depends on the Lorentz factor of the ejecta and their density, and *ii*) its peak flux depends on the total ejecta mass having entered the reverse-shock. Thus, the calculation of the reverse-shock emission requires at least two parameters that quantify the energy and mass injection into the blast-wave, leading to a model even less constrainable (observationally) than the forward-shock (which requires only one parameter,  $e$ , for the energy injection law).

## 5 CONCLUSIONS

By comparing the flux decay index ( $\alpha$ ) with the spectral slope ( $\beta$ ) measured for a set of 98 well-sampled Swift X-ray afterglows with the expectations for the forward-shock model, we find that about a third of those afterglows display a break that could be the traditional ‘jet-break’ claimed to have been observed in a dozen pre-Swift optical afterglows (§2.3.1). For this test of *adiabatic* jet-breaks, we have considered various details of the forward-shock model: homogeneous or wind-like ambient media, spectral cooling frequency higher or lower than the X-rays, synchrotron or inverse-Compton as the dominant X-ray process, a collimated conical or spreading outflow.

If a steady energy injection into the forward-shock occurs, then the jet-break model may account for 88 percent of the 117 light-curve breaks or, else put, for at least one break in 87 percent of the 98 afterglows selected here (§3.3.1). This vast improvement over the adiabatic jet model suggests that energy injection could be a prevalent process in GRB afterglows.

The remaining 12 percent of breaks that cannot be explained by a jet-break undergoing a steady energy injection, and the 19 afterglows with two breaks (only one being, at most, a jet-break), indicate that some X-ray breaks may originate from a change in the rate at which energy is added to the forward-shock (an energy-injection break), and it is possible that some (many ?) of the identified jet-breaks are also energy-injection breaks (§3.3.2). It should be recognized that the complete success of the energy-injection break model over the traditional jet-break model could be due mostly to that the latter model is over-constrained (observations provide two constraints: flux pre- and post-break power-law decay indices – for one model parameter: the energy injection power-law exponent), while the former model is not.

We find a tentative correlation between the GRB output and the afterglow X-ray flux decay rate, more energetic bursts being followed by faster decaying afterglows (§4.1). If energy injection is a common process in GRB afterglows, then the slower decaying afterglows should be identified with a stronger total energy injection. This means that the GRB energy – afterglow (X-ray flux) decay rate correlation should lead to an anticorrelation of the GRB output with the increase of the outflow kinetic energy during the afterglow phase, i.e. more energetic bursts should be followed by afterglows with less energy being injected. This anticorrelation is, indeed, observed for both the jet-break and the energy injection break models for X-ray light-curve breaks, and for various model details (dynamics, X-ray afterglow emission process, radial stratification of the ambient medium). If the GRB progenitor is a long-lived source of relativistic ejecta, the above anticorrelation implies an anticorrelation of the kinetic energy of the leading outflow (producing the burst) with that of the following ejecta (which inject energy in the blast-wave during the afterglow phase), but the total ejecta energy (burst plus afterglow) is far from being universal.

The energy budget required by most of the possible variants of the forward-shock model ranges from  $10^{49}$  to  $10^{52}$  ergs, and only variants involving inverse-Compton emission in the X-rays and a wind-like medium can be excluded on

energetic grounds because, in those models, the required jet-energy exceeds  $10^{53}$  erg (§4.2). Considering both models for light-curve breaks (jet-break with steady energy-injection and energy-injection break), we find that the most energetically economical model is that of a narrow jet whose jet-break occurs early on (before first X-ray measurement) with the light-curve break being an energy-injection break, followed by a model where the X-ray light-curve break is a jet-break, with the most "wasteful" model being that of a wide jet whose break occurs late (after last X-ray measurement), the X-ray break being an energy-injection break. However, the average (over afterglows) energy ratio among pairs of these three break models is only 2–3.

## ACKNOWLEDGMENTS

This work was supported by an award from the Laboratory Directed Research and Development program at the Los Alamos National Laboratory and made use of data supplied by the UK Science Data Center at the University of Leicester, by the "GRB log" site for optical light-curves (<http://grblog.org/grblog.php>), and by the GRB afterglow repository of GCN circulars (<http://www.mpe.mpg.de/~jcg/grbgen.html>).

## REFERENCES

- Chevalier R., Li Z., Fransson C., 2004, *ApJ*, 606, 369  
 Chincarini G. et al, 2007, *ApJ*, 671, 1903  
 Curran P. et al, 2009, *MNRAS*, 395, 580  
 Evans E. et al, 2007, *A&A*, 469, 379  
 Evans E. et al, 2009, *MNRAS*, 397, 1177  
 Falcone A. et al, 2007, *ApJ*, 671, 1921  
 Ghisellini G., Ghirlanda G., Nava L., 2007, *ApJ*, 658, L75  
 Hawley J. & Krolik J., 2006, *ApJ*, 641, 103  
 Ioka K. et al, 2006, *A&A* 458, 7  
 Kumar P., Panaitescu A., 2000, *ApJ*, 541, L9  
 Liang E., Zhang B.-B., Zhang B., 2007, *ApJ*, 670, 565  
 Liang E. et al, 2008, *ApJ*, 675, 528  
 van Marle A. et al, 2006, *A&A*, 460, 105  
 Maxham A. & Zhang B., 2009, *ApJ*, 707, 1623  
 McKinney J., 2005, *ApJ*, 630, L5  
 Mészáros P. & Rees M., 1997, *ApJ*, 476, 232  
 Nousek J. et al, 2006, *ApJ*, 642, 389  
 Nugis T. & Lamers H., 2000, *A&A*, 360, 227  
 Panaitescu A., Mészáros P., Rees M., 1998, *ApJ*, 503, 314  
 Panaitescu A. et al, 2006, *MNRAS*, 366, 1357  
 Panaitescu A., 2007, *MNRAS*, 379, 331  
 Panaitescu A., 2008, *MNRAS*, 383, 1143  
 Panaitescu A., 2011, *MNRAS*, 414, 1379  
 Panaitescu A. & Vestrand T., 2011, *MNRAS*, 414, 3537  
 Quimby R., McMahon E., Jeremy M., 2004, "GRBs: 30 years of Discovery", *AIP Conf Proc*, 727, 529  
 Racusin J. et al, 2008, *Nature*, 455, 183  
 Ramirez-Ruiz E. et al, 2005, *ApJ*, 631, 435  
 Rees M. & Mészáros P., 1994, *ApJ*, 430, L93  
 Rees M. & Mészáros P., 1998, *ApJ*, 496, L1  
 Rhoads J., 1999, *ApJ*, 525, 737  
 Sari R. & Piran T., 1995, *ApJ*, 455, L143  
 Uhm Z. & Beloborodov A., 2007, *ApJ*, 665, L93  
 Willingale R. et al, 2007, *ApJ*, 662, 1093  
 Zhang B. et al, 2006, *ApJ*, 642, 354